Scientific Publications

World Journal of Geomatics and Geosciences, 2025, 4, 6101
www.scipublications.com/journal/index.php/wjgg
DOI: 10.31586/wjgg.2025.6101

Article

Geochemistry distributions and statistics analysis of REE in stream sediments from the watershed west of Mambaka (Adamawa Plateau, Cameroun)

Roland William Edima Yana [1,2,*], Lise Carole Okomo Atouba [3], Fagny Aminatou Mefire [2], Oumar Hamit Djiddi [2], Adama Haman [2], Anicet Ango Ella [2], Faarouk Oumarou Nkouandou [2]

[1] Centre for Geological and Mining Research, Garoua, Cameroon
[2] Department of Earth Sciences, Faculty of Sciences, University of Ngaoundere, Nga-oundere, Cameroon
[3] Higher Teacher Training College of Bertoua, University of Ngaoundere, Bertoua, Cameroon

*Correspondence: Roland William Edima Yana (yanawilliam123@gmail.com)

Abstract: The Mambaka watershed is extends between latitudes 1 3°45'E and 14°15'E and longitudes 7°16'N and 6°45'N. The geology, various tectonic and structural events that have affected the Adamawa Plateau in Cameroon make it rich in multi-substance mining. The objective of this study is to map rare earth (REE) geochemical anomalies in the sediments of the watershed streams west of Mambaka, and to trace their origins and geochemical processes. Predictive maps from inverse distance interpolations (IDW), factor analysis (F1) or principal component analysis (PCA) and hierarchical bottom-up classification maps provided a better understanding of the central tendency, distribution and dispersion of REE in the samples and in the study area, based on standard deviation and variance values that generated two factors F1 (Ho-Tm-Er-Yb-Lu-Dy-Tb-Gd-Eu-Sm) and F2 (Pr-Nd-Ce-La-Sm) representing 92.44% of the total cumulative variance. The ratios Ce/Ce* > 0.78 and Eu/Eu* > 1 demonstrate positive anomalies in Ce and Eu, and clear differentiation. The normalized concentrations used to calculate fractionation ratios show that the values for LaN/YbN (0.58 to 1.34), LaN/SmN (0.61 to 0.88) and LaN/LuN (0.62 to 1.43) suggest higher fractionation in SS09 and lower fractionation in SS01. Similarly, the ratios La/Lu (61.71 to 143.46), La/Yb (9.00 to 20.72), La/Sm (4.02 to 5.83) and La/ Lu (61.71 to 143.46) confirm these higher ratios in SS09 and lower in SS01. The REE in the study area comes from hydrothermal processes based on high lineament densities at sampling points in igneous rocks with a mean ∑REE value of between 174-219 ppm.

Keywords: Geochemical prospecting, Rare earths, Stream sediments, Anomaly, Watershed, Mambaka

How to cite this paper:
Edima Yana, R. W., Okomo Atouba, L. C., Mefire, F. A., Hamit, O. D., Haman, A., Ella, A. A., & Nkouandou, F. O. (2025). Geochemistry distributions and statistics analysis of REE in stream sediments from the watershed west of Mambaka (Adamawa Plateau, Cameroun). *World Journal of Geomatics and Geosciences, 4*(1), 12–28.
DOI: 10.31586/wjgg.2025.6101

Received: October 21, 2024
Revised: April 9, 2025
Accepted: May 7, 2025
Published: May 13, 2025

1. Introduction

Rare earth elements (REE) are defined as a group of 17 transition metals including the 15 lanthanides, atomic numbers 57 to 71 are sometimes added, according to IUPAC (International Union of Pure and Applied Chemistry). The lanthanides (La - Lu) form an extremely coherent family in terms of their chemical properties. Yttrium (Y) has an ionic radius close to that of Holmium (Ho) and is generally associated with the lanthanides, which is not the case for Scandium (Sc), which is rarely distributed in the same phases as the lanthanides in the natural environment. The lanthanide + yttrium group is sometimes referred to by the acronym REY. In this study, the term rare earths (REE) refers to the lanthanides, but Scandium (Sc), Yttrium (Y) and Promethium (Pm) will not be studied in this work. A distinction is usually made between light rare earths (LREE), from Lanthanum (La) to Gadolinium (Gd), and heavy rare earths (HREE), from Terbium (Tb)

to Lutetium (Lu) with Yttrium (Y), as defined by the International Union of Pure and Applied Chemistry (IUPAC). Medium rare earths (MREE), for middle REE, are also used to designate rare earths (REE) from Samarium (Sm) to Dysprosium (Dy). This group distinction also varies according to the authors, the terrain studied, the environment studied, etc [1]. Among processes, rare earths can be used to trace hydrothermal events [2], diagenesis [3] or the mode of formation of different materials (formation of different materials [4,5,6,7]. More rarely, they have been used as tracers in pedogenesis [8].

However, the aim of geochemical prospecting is to: Locate primary dispersal aureoles by studying the distribution of chemical elements in the deposit's host rocks; locate so-called secondary dispersal aureoles and high-grade zones that develop along watercourses in stream sediments and on mountain slopes, by studying the distribution of elements in soil and stream sediments. For this reason, stream sediments are the most widely used sampling media for regional geochemical studies around the world for the delineation of potentially mineralized zones (anomaly detection), but also for the definition of basic geochemical conditions (the baseline analysis, [9]). In addition, they can locate areas contaminated by anthropogenic factors [10]. This work makes a contribution to the identification of rare earth geochemical anomalies, their origin, formation processes and associations in stream sediments in the west of the Mambaka watershed in Nyambaka locality (south of Ngaoundéré).

The Mambaka extends between latitudes 1 3°45'E and 14°15'E and longitudes 7°16'N and 6°45'N watershed It is bounded by the villages of Mbidou to the north, Néminaka to the south and Malam Héman to the west, and by the edge of the Mayo Sokandé watershed to the east (Figure 1 c).

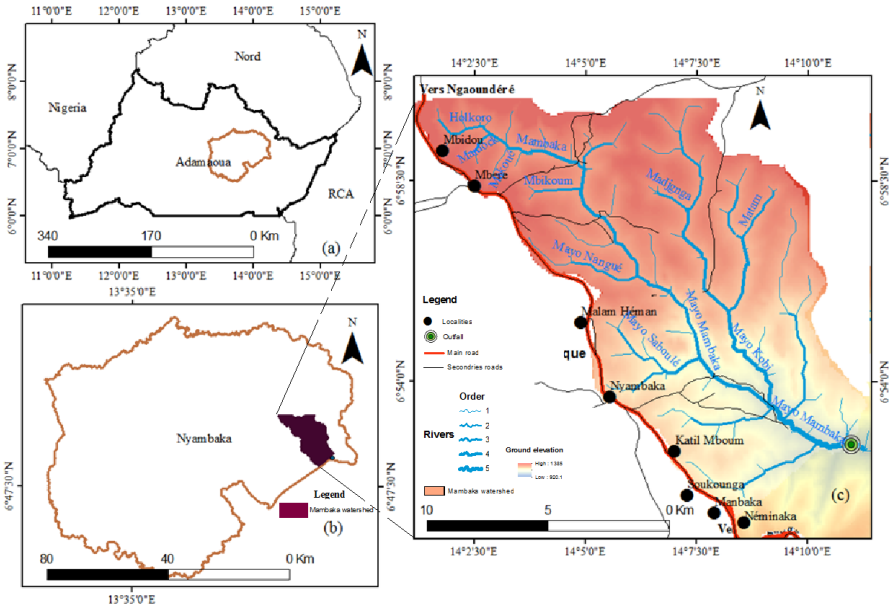

Figure 1. Map showing location of study area: (a) Nyambaka in Adamawa; (b) Nyambaka study area; (c) Mambaka watershed.

The altitude of the area varies from 920 m to over 1,385 m. The upper north is the area with the highest altitudes, covered with rounded or sub-ovoid hills and covered in places by basalt. Slopes at river and stream level are steep, ranging from 3.53% to 14.47%.

The Adamawa Plateau is part of the central domain of the Central African Orogenic Chain (COAC) [11]. In Cameroon, it is assimilated to a volcano-tectonic horst of Cenozoic age with an average altitude of 1000 m, bounded to the north by the Ngaoundéré fault and to the south by the Mbéré fault [12]. The horst consists of Precambrian metacratonic

blocks located at different altitudes and bounded by ductile shears running NE-SE, N70E and N130°-140° [13,14,15]. More or less deformed granitoids of Pan-African age [16,17] are emplaced in orthogneisses and schists of Paleoproterozoic to Neoproterozoic age [18,19,20]. It is a basement cut by numerous faults [21,22] and overlain in some places by sedimentary formations of Cretaceous age and volcanic formations of Cenozoic age [23,24,25]. The main discontinuity crossing the Adamaoua Plateau is the Central African Shear (ZCAC), which extends some 2000 km to Sudan [21]. A structural study carried out on the northern and southern edges of the plateau [12] highlights: (1) a WNW-ESE shortening phase (P1), in a strike-slip regime that brings the N70°E-trending Pan-African mylonitic faults corresponding to the Central African shears into play in dextral sliding [26], (2) a distensive phase (P2) NNE-SSW and (3) a compressive phase (P3) NW-SE. Submeridian distension in the Cenozoic facilitated the surrection of the Adamaoua horsts with volcanic activity and accentuated the collapse of the Djérém and Mbéré troughs [27] (Figure 2 a, b).

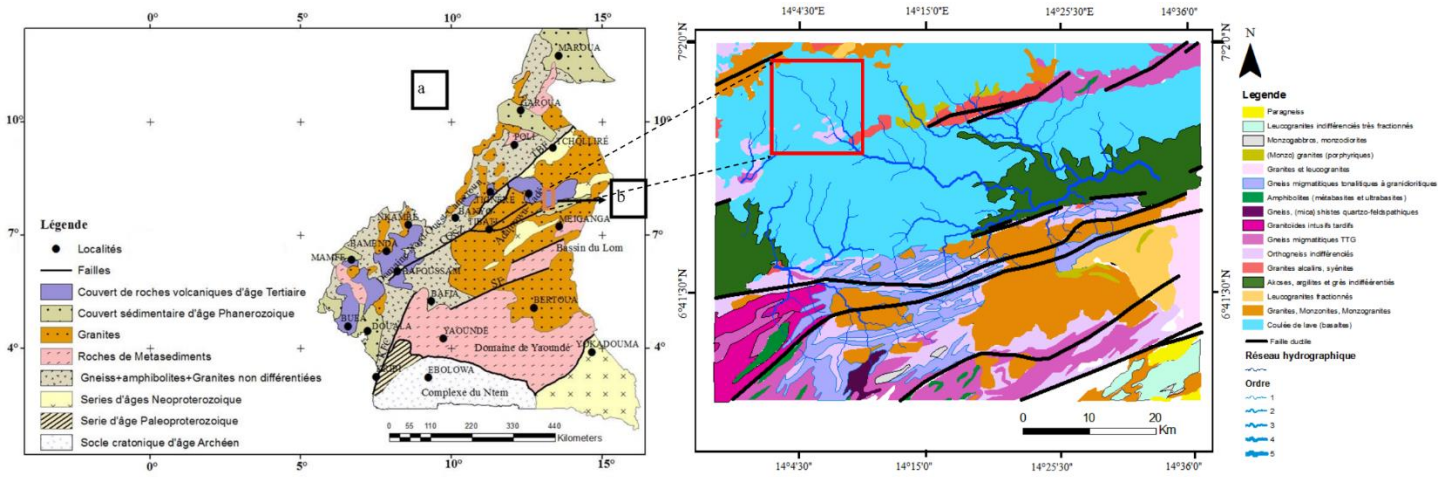

Figure 2. a) Geological map of Cameroon from [28]; b) geological map of the study area.

Studies on the mineralization of gold, tin, tungsten and other metallic substances have already been carried out in certain areas of this vast domain in rocks, soils, alluvium, laterites and stream sediments [29,30,31,32,33,34,35,36], etc.) and some are currently being studied. Spot gold anomalies with grades ranging from 2.20 to 30.30 ppb were revealed on the five sheets explored (Ngaoundéré, Tignère, Bagodo, Tibati and Banyo). In the Nyambaka study area, work by [35] revealed anomalous zones or mineralization grouped according to five (5) factors after multivariate statistical analysis: Sc-Mo-V-In-Ga-Cu-Cr-Ba-Sr-Ag-Cu-Co-Be-Ni-Y-Zn-V,Ga-Hf-Zr,Sn-Au and As-Cd. These anomalies have been identified in the same watershed that is the subject of this study. Similarly, work by [36] in the watershed south of the commune of Nyambaka, revealed the presence of high concentrations of certain elements: Co, Cr, Cu, Ni, En, Y, Ga, La, Sn, Sc, Ce, and rare earth elements.

2. Materials and Methods

2.1. Data Collection and Analysis of Stream sediment

Stream sediment samples were collected following the protocol (published by Fordyce et al. 2022) and avoiding any anthropogenic contamination (Figure 3). Theoretical points were tracked using GPS, and once the theoretical point had been found, the coordinates of the practical sampling points were taken with precision. At the practical sampling point, around 5 kg (to ensure fine-grained material was available for analysis) of stream sediment was collected at a depth of around 15cm. A total of ten (10) stream

sediment samples were collected from the banks of drained or dewatered streams. Samples were described in the field using a geochemical data sheet.

In the laboratory, the wet stream sediment samples collected were poured into clean stainless steel plates, labelled and dried first in the greenhouse, at the Laboratoire de Traitement des Minerais (LTM) de Nkolbisson of the Institut de Recherches Géologiques et Minières (I.R.G.M) in Yaoundé. Samples were ground in a mortar grinder (FRITSCH pulverisette), then 20 g of powder fraction was collected after passing through a 0.75 µm sieve. The collected powder fraction was packaged, labelled and shipped from the Bureau Véritas laboratory in Vancouver, Canada. Stream sediment samples were dried at a lower temperature of 60°C / 140°F, sieved to -180 micron (80 mesh). The 20g powder fractions were analyzed by ICP-MS (Inductivily Coupled Plasma Mass Spectrometry) performed at the "Geological Rock Samples for analysis to Bureau veritas commodities Ltd" laboratory in Vancouver, Canada after modified aqua regia digestion (1: 3: 1 HNO3: HCl: H2O) for ultra-low sediment determinations. Larger slits (20 g) gave a more representative result for the analysis of elements subject to a nugget effect (e.g. Au), as the gold solubility of the samples may be limited in refractories and graphite. A total of 14 rare earth elements from stream sediments out of 20g sample (La, Ce, Pr, Nd, Sm, Eu, Gd, Tb, Dy, Ho, Er, Tm, Yb, Lu) were analyzed. . Quality control (QC) was carried out on a duplicate sample with identical chemical element results. Geochemical data were spatially represented as part of distribution maps, which plot the occurrence of geochemical elements superimposed on drainage, for the geochemical research area. Each sample was assigned an identifier to represent its catchment area. The maps were produced using ArcGis 10.5. The geographic coordinate system used in the study area is DATUM: WGS84. It was used for gridding and plotting the data. The standard deviation from the mean of the grouped data was used to assign color intensities to the maps, as it highlights the contrast between high and low values of the mean. The Pearson correlation coefficient between average rare earth concentration in the watershed and descriptive and multivariate statistical analysis was performed using IBM SPSS Statistics 21.

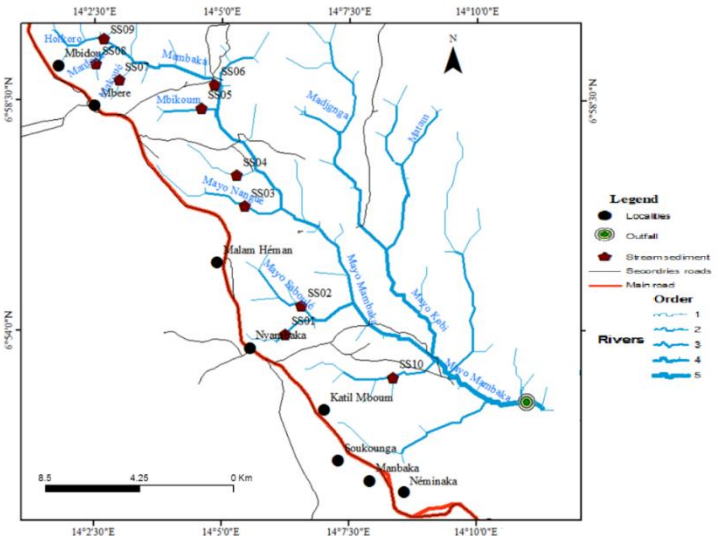

Figure 3. Stream sediment sampling map.

2.2. Data Processing

Traditional statistics here refer to univariate analysis for the calculation of mean and standard deviation. The parameters involved: minimum, mean, maximum, standard deviation, skewness and kurtosis of geochemical element concentrations, which clearly presents the characteristics of the frequency distribution of the geochemical elements

studied. In this study the Asymmetry standard Error is 0.687 and the Kurtosis standard Error: 1.334.

3. Results

Graphical analysis of the histograms shows the dispersion and distribution of REE in the western Mambaka watershed. The central tendency applied here is the mean and the geochemical data of the lognormal distribution were obtained after application of logtransformation. Box-plots can be used to visualize concepts such as the symmetry, dispersion or centrality of the distribution of values associated with a variable. All values were calculated from data grouped and centered around the medians of the ETRs. Pearson correlation coefficients are shown in Table 1. Only coefficients for chemical elements with a strong correlation have been bolded according to the degree of significance. The LREE have strong correlation with all the LREE and the values range from 0.59 to 0.97. The HREE have strong correlation with all the LREE and the values range from 0.51 to 0.99.

Table 1. Correlation of Pearson's

	La	Ce	Pr	Nd	Sm	Eu	Gd	Tb	Dy	Ho	Er	Tm	Yb	Lu
La	1													
Ce	**0,59**	1												
Pr	**0,97**	**0,75**	1											
Nd	**0,89**	**0,77**	**0,95**	1										
Sm	**0,67**	**0,66**	**0,75**	**0,90**	1									
Eu	0,07	0,05	0,10	0,35	**0,68**	1								
Gd	0,44	0,23	0,44	**0,66**	**0,85**	**0,87**	1							
Tb	0,43	0,19	0,43	**0,64**	**0,84**	**0,87**	**0,99**	1						
Dy	0,30	-0,02	0,27	0,48	**0,67**	**0,81**	**0,94**	**0,96**	1					
Ho	0,21	-0,15	0,17	0,37	**0,57**	**0,77**	**0,88**	**0,91**	**0,98**	1				
Er	0,20	-0,20	0,14	0,32	**0,50**	**0,70**	**0,84**	**0,87**	**0,96**	**0,99**	1			
Tm	0,18	-0,21	0,13	0,32	**0,51**	**0,71**	**0,83**	**0,86**	**0,95**	**0,99**	**0,99**	1		
Yb	0,12	-0,32	0,05	0,22	0,40	**0,67**	**0,77**	**0,81**	**0,92**	**0,97**	**0,98**	**0,98**	1	
Lu	0,01	-0,40	-0,05	0,11	0,32	**0,66**	**0,73**	**0,76**	**0,90**	**0,95**	**0,96**	**0,97**	**0,98**	1

Multivariate statistics are well-known approaches to the analysis of prospecting and geochemical exploration data. They define mathematical measures for understanding the interdependence between variables and their relevance to the problem under study [37,38]. Various multivariate statistics, including principal component analysis (PCA) [39], factor analysis (FA) [40] and distance interpolation method (IDW) are effective for extracting multivariate geochemical anomalies related to mineralization [41,42,43,44,45,46]. The rotated space component plot was extracted using the rotation method: Verimax with Kaiser Normalization. This diagram shows two groups of rare earth elements along two axes PC1 and PC2. This analysis shows that PC1 groups heavy rare earths (HREE) and PC2 light rare earths (LREE) (Figure 4).

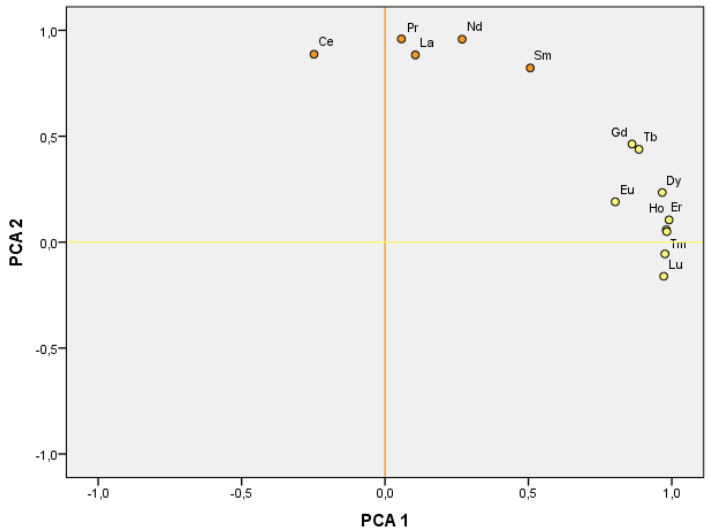

Figure 4. Two groups of rare earth elements along two axes PC1 and PC2 after Principals Component Analysis (PCA)

The hierarchical tree of rare earth element values reveals groups using barycenter distance and interval measure: Pearson correlation. The first group shows a heavy rare earth association (HREE) and the second a light rare earth association (LREE). These groups of rare earth elements show two major lithogeochemical ensembles. The hierarchical ascending classification represented by the hierarchical tree of observations shows the resized classes of stream sediment samples by the aggregation method using the distance of barycenters and interval measurement: Pearson correlation.

Interpolation of geochemical exploration point data into raster maps is a routine process for processing geochemical exploration data. As part of this study, inverse distance interpolation (IDW) predictive maps of all REEs were drawn up (Figure 111). These IDW are represented by four subdivided contours in ascending order of interpolation intensity following the colors green, lime green, yellow and red respectively. Interpolation maps for the FAC_1 and FAC_2 factors have also been drawn, and are represented by nine subdivided contours in ascending order of interpolation intensity following the colors green (lower value) to red (higher value) respectively (Figure 5 A,B).

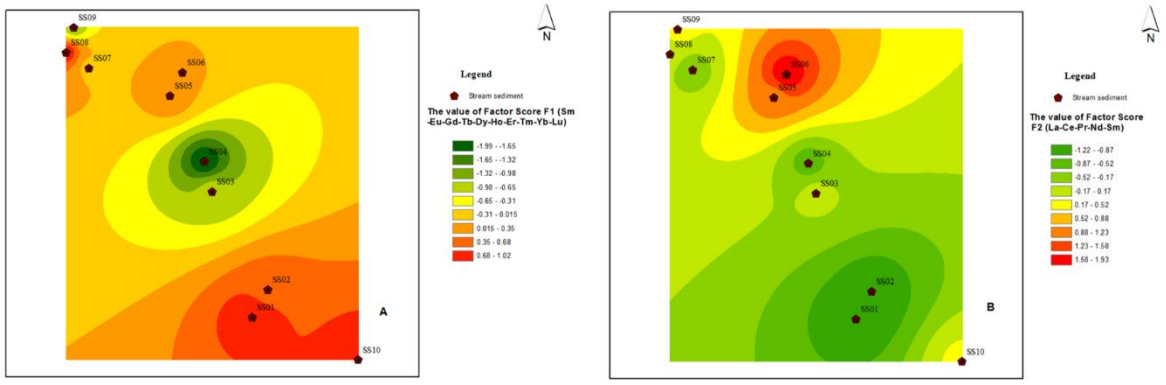

Figure 5. Maps : A) The value of factor score F1; B) The value of factor score F2

The rare earth concentrations of heavy minerals are shown on the rare earth spectra (REE) diagram after Rudnick and Gao 2003 revised 2014. They show more or less parallel trends (Figure 6). The REE trends of these minerals indicate that they come from the same source or belong to similar source rocks. The diagram shows light rare earth enrichment (LREE) and heavy rare earth depletion (HREE) indicating the presence of zircon and with a typical positive Europium anomaly, which is a common feature of magmas crystallizing plagioclase, most of the Europium will be incorporated into this mineral. The rest of the magma will then be relatively low in Europium. Table 2 shows the enrichment of the rare earth elements included in the samples, compared to the Clark (UCC). The Eu_N shows a double ratio in the samples SS01, SS05, SS08 and SS10. The Ce_N shows a double ratio in two samples SS05 and SS06.

Table 2. Rare earth normalization (REE) of stream sediments relative to upper crust from [47] (A: Ce anomaly = 2 × (Ce/Ce_N) / (La/La_N+Pr/Pr_N) And B: Eu anomaly = 2 × (Eu/Eu_N) / (Sm/Sm_N+Gd/Gd_N))

	SS01	SS02	SS03	SS04	SS05	SS06	SS07	SS08	SS09	SS10	Clark (UCC)
La_N	0,82	0,85	0,94	0,77	**1,02**	**1,40**	0,91	0,96	**1,20**	**1,15**	31
Ce_N	**1,25**	**1,22**	**1,65**	**1,57**	**2,01**	**2,01**	**1,55**	**1,60**	**1,64**	**1,41**	63
Pr_N	**1,00**	**1,03**	**1,20**	**1,01**	**1,32**	**1,64**	**1,10**	**1,22**	**1,37**	**1,29**	7,1
Nd_N	**1,06**	**1,03**	**1,15**	**0,98**	**1,37**	**1,54**	**1,09**	**1,21**	**1,22**	**1,27**	27
Sm_N	**1,34**	**1,33**	**1,41**	**1,20**	**1,77**	**1,74**	**1,37**	**1,59**	**1,36**	**1,62**	4,7
Eu_N	**2,08**	**1,87**	**1,82**	**1,60**	**2,38**	**1,93**	**1,98**	**2,28**	**1,47**	**2,48**	1
Gd_N	**1,55**	**1,43**	**1,31**	**1,07**	**1,74**	**1,64**	**1,46**	**1,61**	**1,30**	**1,72**	4
Tb_N	**1,27**	**1,21**	**1,10**	0,90	**1,40**	**1,36**	**1,20**	**1,34**	**1,07**	**1,41**	0,7
Dy_N	**1,44**	**1,31**	**1,13**	0,84	**1,41**	**1,37**	**1,26**	**1,43**	**1,12**	**1,46**	3,9
Ho_N	**1,31**	**1,23**	0,95	0,71	**1,20**	**1,20**	**1,10**	**1,34**	0,96	**1,30**	0,83
Er_N	**1,31**	**1,23**	0,92	0,62	**1,13**	**1,20**	**1,11**	**1,30**	0,93	**1,26**	2,3
Tm_N	**1,43**	**1,37**	0,97	0,60	**1,23**	**1,27**	**1,10**	**1,47**	0,97	**1,37**	0,3
Yb_N	**1,41**	**1,25**	0,90	0,60	**1,05**	**1,17**	**1,08**	**1,36**	0,90	**1,30**	2
Lu_N	**1,32**	**1,23**	0,84	0,55	1,00	1,00	1,00	**1,29**	0,84	**1,19**	0,31
A	3,30	3,32	3,30	3,31	3,30	3,29	3,31	3,31	3,29	3,31	
B	0,23	0,23	0,23	0,22	0,23	0,23	0,22	0,23	0,22	0,22	

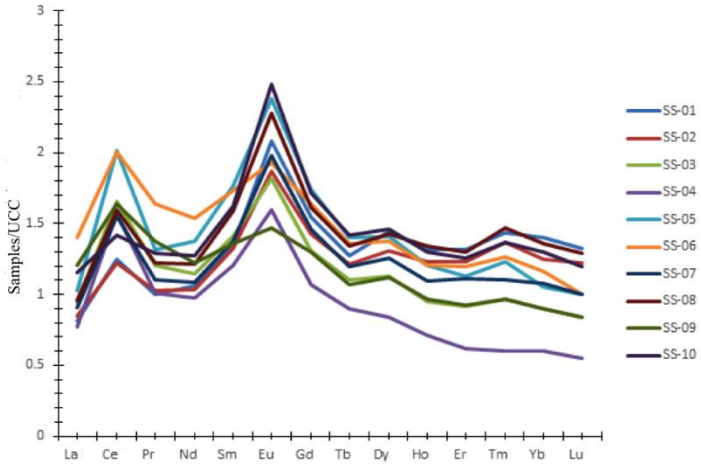

Figure 6. Standardized rare earth spectra [47]

Rare earth models can identify contrasting concentrations of light rare earths versus heavy rare earths, or a relative concentration or depletion of Cerium (Ce) or Europium (Eu). These differences are called fractionation and anomalies respectively, and are quantified using ratios. Geochemical parameters such as Cerium and Europium in sedimentary rocks can be used to judge the source of materials and the sedimentary environment [48]. For this purpose, a Ce/Ce* value of 0.78 is generally adopted as a reference value to indicate a redox environment (Wright et al. 1987). Normally, Ce/Ce* > 0.78 is a positive anomaly and Ce/Ce* < 0.78 is a negative anomaly; Eu/Eu* > 1 is a positive anomaly and Eu/Eu* < 1 is a negative anomaly [49]. In addition to light rare earths (LREE) and heavy rare earths (HREE), the geochemical parameters Ce/Ce* and Eu/Eu* have shown clear differentiation. In all cases, the concentrations used in the calculation of fractionation ratios are the normalized concentrations. The ratio values for LaN/YbN (0.58 to 1.34), LaN/SmN (0.61 to 0.88), LaN/LuN (0.62 to 1.43 show higher fractionation in SS09 and low fractionation in SS01. Similarly, the ratios La/Lu (61.71 to 143.46), La/Yb (9.00 to 20.72), La/Sm (4.02 to 5.83) and La/ Lu (61.71 to 143.46) confirm these higher ratios in SS09 and lower ratios in SS01 (Table 3).

Table 3. Results of rare earth geochemical analysis of samples

Elements	SS01	SS02	SS03	SS04	SS05	SS06	SS07	SS08	SS09	SS10
La (ppm)	25,3	26,2	29,2	23,8	31,7	43,5	28,1	29,7	37,3	35,7
Ce (ppm)	78,5	76,8	104,2	99,0	126,7	126,4	97,7	100,8	103,3	89,1
Pr (ppm)	7,12	7,29	8,54	7,16	9,34	11,62	7,84	8,66	9,75	9,19
Nd (ppm)	28,67	27,88	30,92	26,37	37,03	41,47	29,41	32,74	33,04	34,36
Sm (ppm)	6,30	6,24	6,61	5,66	8,31	8,16	6,46	7,45	6,40	7,63
Eu (ppm)	2,08	1,87	1,82	1,60	2,38	1,93	1,98	2,28	1,47	2,48
Gd (ppm)	6,19	5,72	5,24	4,29	6,95	6,55	5,85	6,45	5,21	6,87
Tb (ppm)	0,89	0,85	0,77	0,63	0,98	0,95	0,84	0,94	0,75	0,99
Dy (ppm)	5,63	5,09	4,40	3,28	5,51	5,35	4,91	5,58	4,36	5,70
Ho (ppm)	1,09	1,02	0,79	0,59	1,00	1,00	0,91	1,11	0,80	1,08
Er (ppm)	3,02	2,84	2,11	1,43	2,59	2,75	2,55	2,99	2,13	2,89
Tm (ppm)	0,43	0,41	0,29	0,18	0,37	0,38	0,33	0,44	0,29	0,41
Yb (ppm)	2,81	2,49	1,80	1,20	2,10	2,33	2,15	2,71	1,80	2,60

Lu (ppm)	0,41	0,38	0,26	0,17	0,31	0,31	0,31	0,40	0,26	0,37
Ce/Lu	191,46	202,11	400,77	582,35	408,71	407,74	315,16	252,00	397,31	240,81
La/Yb	9,00	10,52	16,22	19,83	15,10	18,67	13,07	10,96	20,72	13,73
La/Sm	4,02	4,20	4,42	4,20	3,81	5,33	4,35	3,99	5,83	4,68
Gd/Yb	2,20	2,30	2,91	3,58	3,31	2,81	2,72	2,38	2,89	2,64
La/Lu	61,71	68,95	112,31	140,00	102,26	140,32	90,65	74,25	143,46	96,49
La_N/Yb_N	0,58	0,68	1,05	1,28	0,97	1,20	0,84	0,71	1,34	0,89
La_N/Sm_N	0,61	0,64	0,67	0,64	0,58	0,81	0,66	0,60	0,88	0,71
Gd_N/Yb_N	1,10	1,15	1,46	1,79	1,65	1,41	1,36	1,19	1,45	1,32
La_N/Lu_N	0,62	0,69	1,12	1,40	1,02	1,40	0,91	0,74	1,43	0,96
ΣLREE (La-Sm)	145,89	144,41	179,47	161,99	213,08	231,15	169,51	179,35	189,79	175,98
ΣHREE (Gd-Lu)	20,47	18,80	15,66	11,77	19,81	19,62	17,85	20,62	15,60	20,91
ΣMREE (Sm-Ho)	22,18	20,79	19,63	16,05	25,13	23,94	20,95	23,81	18,99	24,75
ΣREE	168,44	165,08	196,95	175,36	235,27	252,70	189,34	202,25	206,86	199,37
ΣLREE/ΣHREE	7,13	7,68	11,46	13,76	10,76	11,78	9,50	8,70	12,17	8,42
$(ΣLREE)_N$	5,47	5,45	6,35	5,53	7,49	8,32	6,03	6,58	6,80	6,76
$(ΣHREE)_N$	11,05	10,25	8,11	5,89	10,16	10,20	9,30	11,14	8,09	11,01
$(ΣMREE)_N$	9,00	8,38	7,72	6,33	9,90	9,24	8,37	9,59	7,29	10,00
Eu/Eu*	1,44	1,38	1,36	1,14	1,75	1,69	1,42	1,60	1,33	1,67
Ce/Ce*	1,13	1,14	1,76	1,38	2,33	3,04	1,55	1,73	2,11	1,73

4. Discussion

The average lanthanum (La) content is 31.05 ppm. This is significantly higher than the lanthanum (La) content of the upper continental crust (31 ppm) (Appendix A (a)). The highest content is observed in sample SS06 and the lowest in SS04, both of which occur in a basalt-covered zone (Appendix A). The maximum Lanthanum (La) content is higher than in the watershed south of Nyambaka commune, where the value is 42.40 ppm [36], and lower than in samples NT18 (3122.6 ppm), NT05 (1867.7 ppm) and NT26 (556.8 ppm) studied in stream sediments in the Paleoproterozoic series of the Nyong, South Cameroon [33]. Sample SS06 has a higher content (43.50 ppm) than the North East (32.15 ppm), North (20.39 ppm), West (26.51 ppm) and North West (22.98 ppm) samples from the Baotou mine soils in China [50]. Lanthanum shows a positive Pearson correlation coefficient with Ce, Pr, Nd and Sm. The enrichment observed in the river hosting the sediments of sample SS06, a tributary of Mambaka, as indicated by the inverse distance interpolation predictive maps IDW_ La (Figure 13 a) and IDW_FAC_2, could originate from the basalts and granitoids where the hydrothermal fluids flowed (Appendix B (a)).

The average cerium (Ce) content is 100.25 ppm. This is higher than the Cerium (Ce) content in the upper continental crust (63 ppm). The highest content was observed in sample SS05 and the lowest in SS02, which occur in an area covered by basalts and orthogneiss (Appendix A (b)). The maximum Cerium (Ce) content is higher than in the watershed south of Nyambaka commune, with a value of 115.60 in EY-15 [36]. These Cerium (Ce) element contents are also higher than those of magnetite samples 13D14E09 (0.048 ppm) and 13D14B12 (58.17 ppm) analyzed from the Bayan Obo deposit in northern China [51]. The enrichment observed in the river hosting the sediments of samples SS05

in the Mbikoum River and SS06 tributary of Mambaka, as indicated by the predictive maps IDW_Ce (Appendix B (b)) and IDW_FAC_2, could originate from hydrothermal fluids.

The average Praseodymium (Pr) content is 8.651 ppm. This is higher than the Pr content in the upper continental crust (7.1 ppm) (Appendix A (c)). The highest content was observed in sample SS06 and the lowest in SS01, which are present in a basalt-covered zone. The maximum Pr content is higher than that found in the watershed south of Nyambaka commune, with a value of 10.61 ppm in EY-10 [36] and lower than samples NT18 (598.33 ppm), NT05 (378.34 ppm) and NT26 (118.69 ppm) studied in stream sediments in the Nyong paleoproterozoic series, southern Cameroon [33]. These grades are also higher than those of magnetite samples, except for one sample grading 8.81 ppm analyzed in the Bayan Obo deposit in northern [51]. The enrichment observed in the river hosting the sediments of sample SS06, a tributary of Mambaka, as indicated by the predictive maps IDW_Pr (Appendix B (c)) and IDW_FAC_2, could come from hydrothermal fluids.

The average Neodymium (Nd) content is 32.18 ppm. This is significantly higher than the (Nd) content of the upper continental crust (27 ppm). The highest content is observed in sample SS06 (Appendix A (d)), which occurs in a basalt-covered zone. The maximum Neodymium (Nd) content is higher than in the watershed south of Nyambaka commune, where the value is 40.09 ppm [36] and lower than in samples NT18 (598.33 ppm), NT05 (378.34 ppm) and NT26 (118.69 ppm) studied in stream sediments in the Nyong paleoproterozoic series, southern Cameroon [33]. Pr shows a positive Pearson correlation coefficient with Ce, La, Nd and Sm. The enrichment observed in the rivers hosting the sediments of samples SS05 at the Mbikoum River and SS06 tributary of Mambaka, as indicated by the predictive maps IDW_Nd zones (Figure 13 d) and IDW_FAC_2 (Appendix A (d)), could originate from hydrothermal fluids in the fracturing.

The average Samarium (Sm) content is 6.92 ppm. This is significantly higher than the Samarium (Sm) content in the upper continental crust (4.7 ppm). The highest content is observed in sample SS06 (Appendix A (e)), which occurs in a basalt-covered zone. The maximum Sm content is lower than in the watershed south of Nyambaka commune, where the value is 8.53 ppm [36] and lower than in samples NT18 (598.33 ppm), NT05 (378.34 ppm) and NT26 (118.69 ppm) studied in stream sediments in the Nyong paleoproterozoic series, southern Cameroon [36]. The enrichment observed in the rivers hosting the sediments of samples SS05 in the Mbikoum River and SS06 in the Mambaka tributary, as indicated by predictive maps IDW_Sm (Appendix B (e)) and IDW_FAC_2, could be due to heavy minerals, in this case zircon, derived from the weathering of surrounding rock formations.

The average Gadolinium (Gd) content is 59.32 ppm. This is higher than the Gadolinium (Gd) content in the upper continental crust (4 ppm). The highest content observed in sample SS05 (Appendix A (g)). The enrichment observed in rivers hosting stream sediments as indicated by the IDW_Gd (Appendix B (g)), IDW_FAC_1 inverse distance interpolation could originate from a hydrothermal source and also marking the presence of heavy minerals in this case Zircon associated with Ga and Hf of granitic origin [35].

The average Terbium (Tb) content is 0.859 ppm. This is higher than the Terbium (Tb) content in the upper continental crust (0.7 ppm). The highest Terbium content was observed in samples SS05 and SS10 (Appendix A (h)). The maximum Terbium content is higher than in the watershed south of Nyambaka commune, with a value of 1.16 ppm [36], and lower than in samples NT18 (598.33 ppm), NT05 (378.34 ppm) and NT26 (118.69 ppm) studied in stream sediments in the Paleoproterozoic series of the Nyong, southern Cameroon[33]. These Gd contents are also higher than those of magnetite samples analyzed from the Bayan Obo deposit in northern China [51]. The enrichment observed in stream sediments, as indicated by the IDW_Tb (Appendix B (h)) and IDW_FAC_1

inverse distance interpolation predictive maps, could be due to the presence of major minerals such as potassic feldspars and accessory Zircon associated with Ga and Hf of granitic origin.

The average Dysprosium (Dy) content is 4.98 ppm. This is higher than the Dy content in the upper crust (3.9 ppm). The highest content was observed in samples SS10, SS06 (Appendix A (i)). The maximum Dysprosium (Dy) content is lower than in the watershed south of Nyambaka commune, where the value is 1.16 ppm [36], and lower than in samples NT18 (598.33 ppm), NT05 (378.34 ppm) and NT26 (118.69 ppm) studied in stream sediments in the Paleoproterozoic series of the Nyong, South Cameroon [33]. These Gd contents are also higher than those of magnetite samples analyzed from the Bayan Obo deposit in northern China [51]. The enrichment observed in stream sediments, as indicated by the IDW_Dy and IDW_FAC_1 (Appendix B (i)) inverse distance interpolation predictive maps, could be due to the presence of major minerals such as potassic feldspars

The average Holmium (Ho) content is 0.939 ppm. This is higher than the Ho content in the upper continental crust (0.83 ppm). The highest content was observed in samples SS08, SS10, SS01 (Appendix A (j)). The maximum Ho content is higher than in the watershed south of Nyambaka commune, where the value is 1.29 ppm [36], and lower than in samples NT18 (598.33 ppm), NT05 (378.34 ppm) and NT26 (118.69 ppm) studied in stream sediments in the Paleoproterozoic series of the Nyong, South Cameroon [33]. These Gd contents are also higher than those of magnetite samples analyzed from the Bayan Obo deposit in northern China [51]. The enrichment observed in stream sediments, as indicated by the IDW_Ho (Appendix B (j)), F1 and IDW_FAC_1 could be due to the presence of major minerals such as potassic feldspars, associated Zircon of granitic origin and hydrothermal fluids.

The average Erbium (Er) content is 2.53 ppm. This is higher than the Er content in the upper continental crust (2.3 ppm). The highest content was observed in samples SS01, SS02, SS08 and SS10 (Appendix A (k)). The maximum Er content is lower than in the watershed south of Nyambaka commune, where the value is 3.46 ppm [36], and lower than in samples studied in stream sediments in the Paleoproterozoic series of the Nyong, southern [33]. These Gd contents are also higher than those of magnetite samples analyzed from the Bayan Obo deposit in northern China [51]. The enrichment observed in stream sediments, as indicated by the IDW_Er (Appendix B (k)) and IDW_FAC_1 inverse distance interpolation predictive maps, could be due to the presence of major minerals such as potassic feldspars and accessory Zircon (Ga-Hf-Zr) of granitic origin and hydrothermal fluids in the study area.

The average Thulium (Tm) content is 0.353 ppm. This is higher than the Thulium (Tm) content in the upper continental crust (0.30 ppm). The highest content was observed in samples SS08, SS10, SS02 and SS01 (Appendix A (l)). The maximum Thulium content is higher than that of the watershed south of Nyambaka commune, whose value is 0.44 ppm [36], which can be considered the geochemical threshold, and this content value is lower than the contents of samples studied in stream sediments in the Paleoproterozoic series of the Nyong, South Cameroon [33]. These Gadolinium (Gd) grades are also higher than those of magnetite samples analyzed from the Bayan Obo deposit in northern China [51]. The enrichment observed in stream sediments, as indicated by the IDW_Tm (Appendix B (l)) and IDW_FAC_1 predictive maps, could be due to the presence of major minerals such as potassic and hydrothermal fluids in the study area.

The average Ytterbium (Yb) content is 2.19 ppm. This is higher than the Ytterbium (Yb) content in the upper crust (2 ppm). The highest content was observed in samples SS08, SS10, SS02 and SS01 (Appendix A (m)). The maximum Yb content is lower than that of the watershed south of Nyambaka commune, which has a value of 3.19 ppm [36] and this content value is lower than that of samples studied in stream sediments in the Paleoproterozoic series of the Nyong, South Cameroon [33]. These Gd contents are also

lower than samples selected from ores east of the Fe-Nb-REE-rich carbonate deposit of Bayan Obo and Western Hills in Mongolia, China [52]. The enrichments observed in stream sediments, as indicated by the IDW_Yb (Appendix B (m)) and IDW_FAC_1 inverse distance interpolation predictive maps, could be due to the presence of major accessory minerals, and hydrothermal fluids in the study area.

The average lutetium (Lu) content is 0.318 ppm. This is higher than the Lutetium (Lu) content in the upper continental crust (0.31 ppm). The highest content was observed in samples SS08 and SS01 (Appendix A (n)). The maximum Lutetium content is higher than in the watershed south of Nyambaka commune, where the value is 0.45 ppm [36] and this content value is lower than in samples studied in stream sediments in the Paleoproterozoic series of the Nyong, South Cameroon [33]. These Gd grades are also higher than those of magnetite samples analyzed from the Bayan Obo deposit in northern China [51] and lower than samples selected from ores to the east of the Fe-Nb-REE-rich carbonate deposit of Bayan Obo and Western Hills in Mongolia, China [52]. The enrichment observed in stream sediments, as indicated by the IDW_Lu (Appendix B (n)) and IDW_FAC_1 inverse distance interpolation predictive maps, could be due to the presence of major minerals such as potassic feldspars and accessory minerals, in this case Zircon of granitic origin.

The average Europium (Eu) content is 1.989 ppm. This is higher than the Europium (Eu) content in the upper continental crust (1 ppm). The highest content was observed in samples SS08 and SS05 (Appendix A (f)). The maximum Europium (Eu) content is lower than in the watershed south of Nyambaka commune, where the value is 2.68 ppm [36] and this content value is lower than in samples studied in stream sediments in the Paleoproterozoic series of the Nyong, southern Cameroon [33]. These Eu contents are also higher than those of magnetite samples analyzed from the Bayan Obo deposit in northern China [51]. The enrichment observed in stream sediments as indicated by the IDW_Lu (Appendix B (f)) and IDW_FAC_1 inverse distance interpolation predictive maps could originate from feldspars, which are the only primary silicate minerals to always show a positive Eu anomaly [53,54] due to the replacement of Ca^{2+}, Sr^{2+} and Na^{+} by Eu^{2+} [55] and [56] hence its specific behavior compared to other magnetic rare earths.

4.1. Origin of rare earths in stream sediments

The sum of rare earths ∑REE varies is from 165.08 ppm to 252.7 ppm and average 199.162 ppm. According the concentrations (REE) in the various matrices, this value of average REE is higher than the values of averages in soils (165 mg.kg-1 or ppm) and soil materials from parent rock (178 mg.kg-1 ppm) formed of basic and acidic igneous rocks, sandstones, shales, etc. Samples SS05 and SS06 have high concentrations above 219 ppm and samples SS01, SS02 have concentrations below 174 ppm all ranging from 16 to 700 ppm, except for the remaining samples which have the sum of rare earths ∑REE between 174-219 ppm. So samples SS01, SS02, SS05 and SS06 come from soils, while the rest of the samples come from basic (basalts) and acidic (granites) igneous rocks. Human activities, such as river or groundwater irrigation, phosphorus fertilization and land application of wastes, are also responsible for rare earth (REE) inputs to soils [57]. In my study area, lanthanum levels are in the range 27-45 ppm [58], reflecting phosphogypsium fertilization in the sediments of the study area. This is characterized by the abundance of agricultural and pastoral activities observed near the watercourses sampled in the study area.

5. Conclusion

At the end of this study, the aim was to identify rare earth geochemical anomalies, their origins, their formation processes and their associations that could lead to mineral deposits. The study revealed that stream sediments to the west of the Mambaka watershed contain REEs (light (LREE) and heavy (HREE)) in excess of their content in the upper continental crust. These grades compared to studies carried out in stream sediments in

the Paleoproterozoic series of the Nyong, South Cameroon to the HREE grades of magnetite samples analyzed from the Bayan Obo deposit in Northern China and to samples selected from ores in the eastern part of the Fe-Nb-REE-rich carbonate deposits of Bayan Obo and Western Hills in Mongolia, China provide ample evidence of the relevance of these data in situating positive REE anomalies in the sub-regional, regional and global arena. The ratios Ce/Ce* > 0.78 and Eu/Eu* > 1 demonstrate positive anomalies in Ce and Eu, and clear differentiation. Lanthanum levels in the study area are in the 27-45 ppm range, reflecting phosphogypsium fertilization in the sediments of the study area. This is characterized by the abundance of agricultural and pastoral activities observed near the watercourses sampled in the study area. This represents a major anthropogenic source of rare earths in stream sediments. The normalized concentrations used to calculate fractionation ratios show LaN/YbN, LaN/SmN and LaN/LuN ratios that suggest higher fractionation in SS09 and lower fractionation in SS01. Similarly, the ratios La/Lu, La/Yb, La/Sm and La/ Lu confirm these higher ratios in SS09 and lower in SS01. Predictive maps of distance interpolations (IDW), factorial analysis (FA or F1) or principal component analysis (PCA) and hierarchical bottom-up classification maps provided a better understanding of the distribution and dispersion of rare earths in the samples and in the study area, based on standard deviation and variance values that generated two factors F1 (Ho-Tm-Er-Yb-Lu-Dy-Tb-Gd-Eu-Sm and F2 (Pr-Nd-Ce-La-Sm) representing 92.44% of the total cumulative variance. The REE formation or emplacement processes in the study area result: either from hydrothermal processes relying on the high lineament densities at the sampling points associated with the high correlation coefficients between light rare earths, or come from soils, basalts and granites igneous rocks. The (La/Yb) N values suggest a heterogeneous sorting effect of heavy minerals with variable enrichment of dense, resistant minerals.

Acknowledgements

I would like to thank M. Edima Nathanael, Oyono Amelie Majolie, Ngbwa Emile, Afana Mbono Cecile Flore, Bureau Veritas commodities Canada LTD and the population of the Nyambaka District. This study was funded by M. Edima Yana Roland William and the family.

Funding declaration

Funding was provided by the first author; this work is a part of his thesis.

Declaration of Conflicts of interest/Competing interests

The authors declare that they have known competing financial interest or personal relationships that could have appeared to influence the work reported in this paper.

Appendix

Appendix A: Rare earth elements distribution maps: (a) La, (b) Ce, (c) Pr, (d) Nd, (e) Sm, (f) Eu, (g) Gd, (h) Dy, (i) Tb, (j) Er, (k) Ho,(l) Tm, (m) Yb, (n) Lu

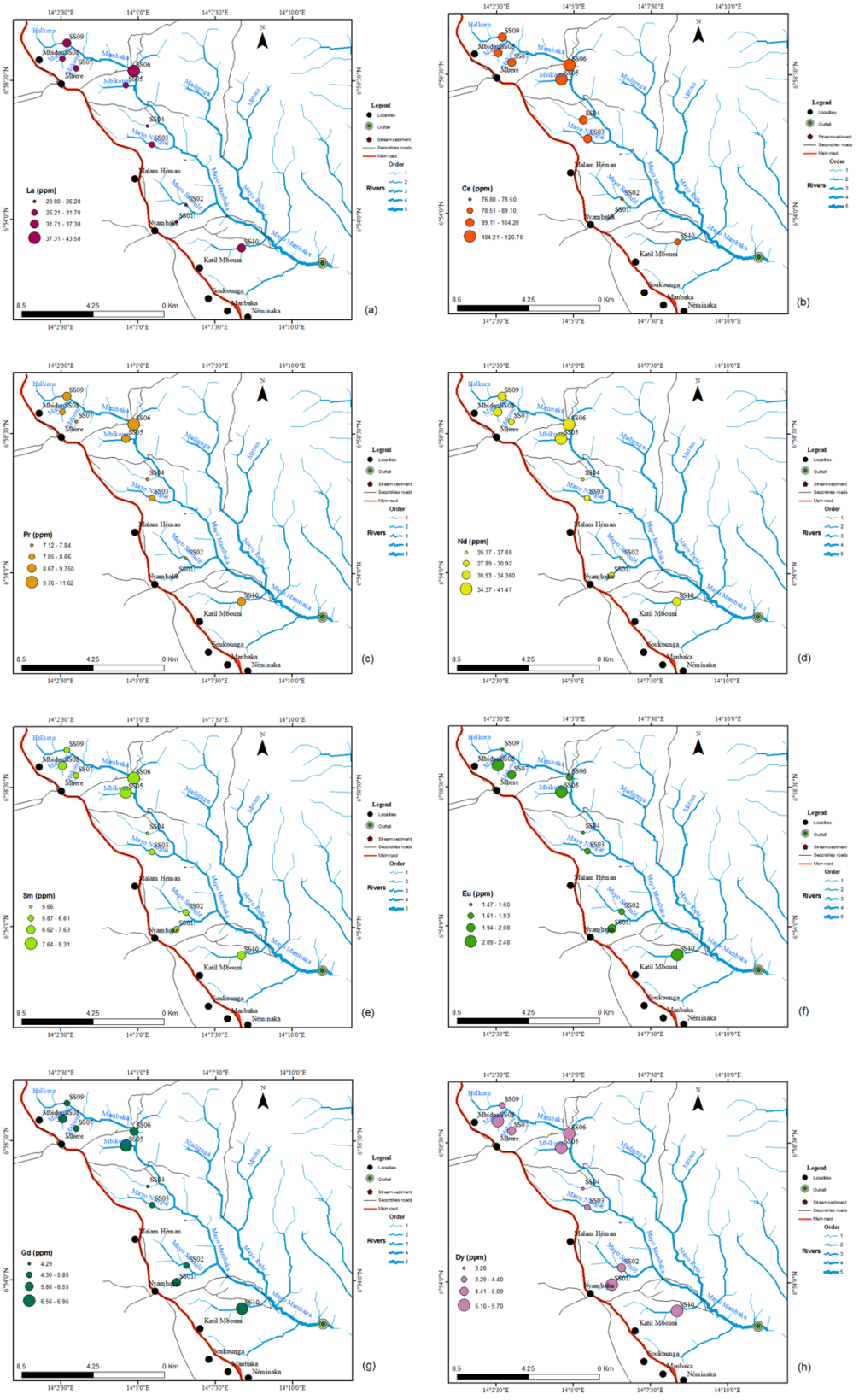

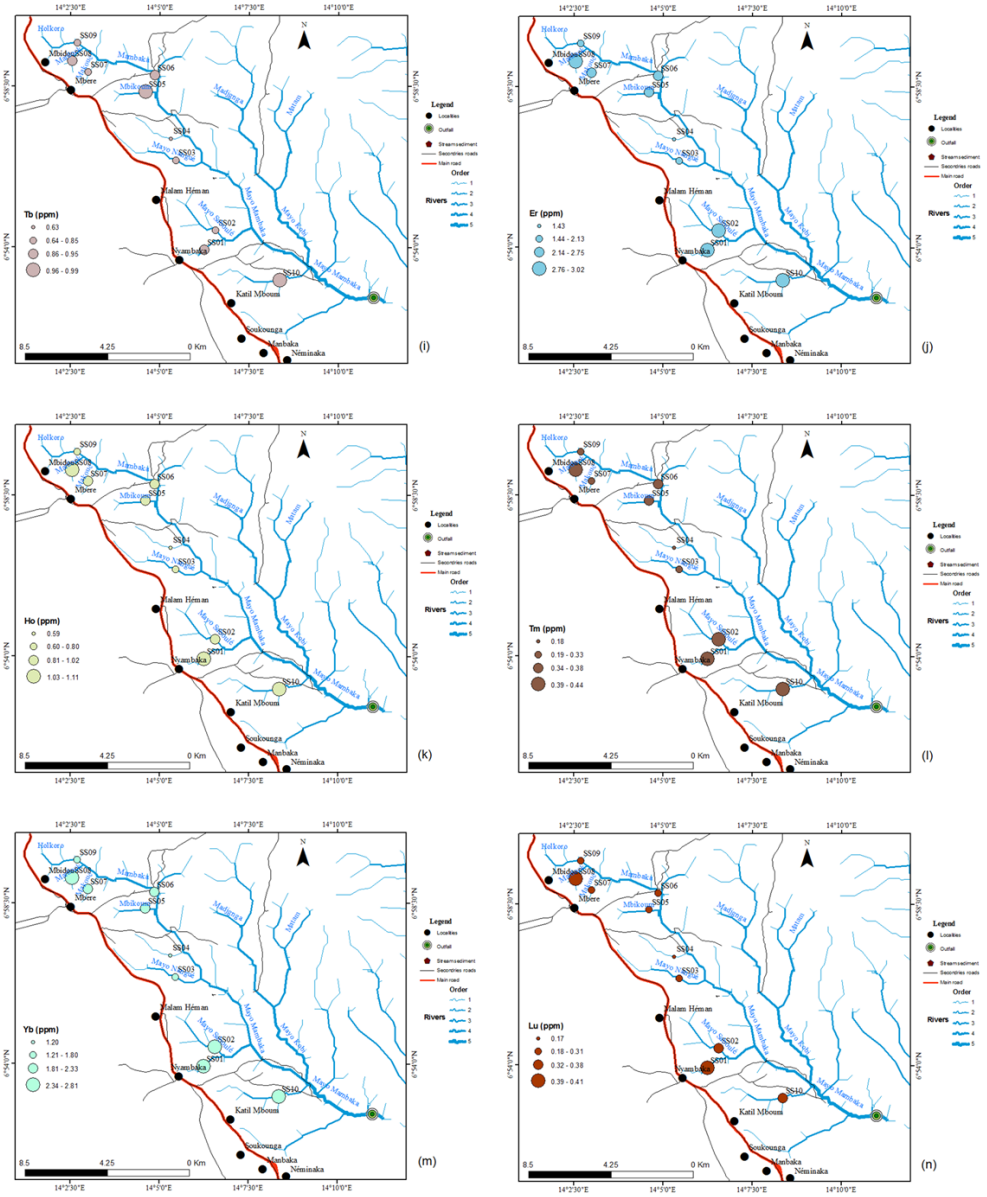
Tb (ppm)
0.63
0.64 - 0.85
0.86 - 0.95
0.96 - 0.99
(i)
Er (ppm)
1.43
1.44 - 2.13
2.14 - 2.75
2.76 - 3.02
(j)
Ho (ppm)
0.59
0.60 - 0.80
0.81 - 1.02
1.03 - 1.11
(k)
Tm (ppm)
0.18
0.19 - 0.33
0.34 - 0.38
0.39 - 0.44
(l)
Yb (ppm)
1.20
1.21 - 1.80
1.81 - 2.33
2.34 - 2.81
(m)
Lu (ppm)
0.17
0.18 - 0.31
0.32 - 0.38
0.39 - 0.41
(n)
Ndokop
Mbere
Ndjam Héman
Nyambaka
Katil Mbouna
Soukounga
Mambaka
Nèmimaka
Legend
Rivers
Order
0 Km

Appendix B: Distance interpolation maps (IDW) : (a) La, (b) Ce, (c) Pr, (d) Nd, (e) Sm, (f) Eu, (g) Gd, (h) Dy, (i) Tb, (j) Er, (k) Ho, (l) Tm, (m) Yb, (n) Lu

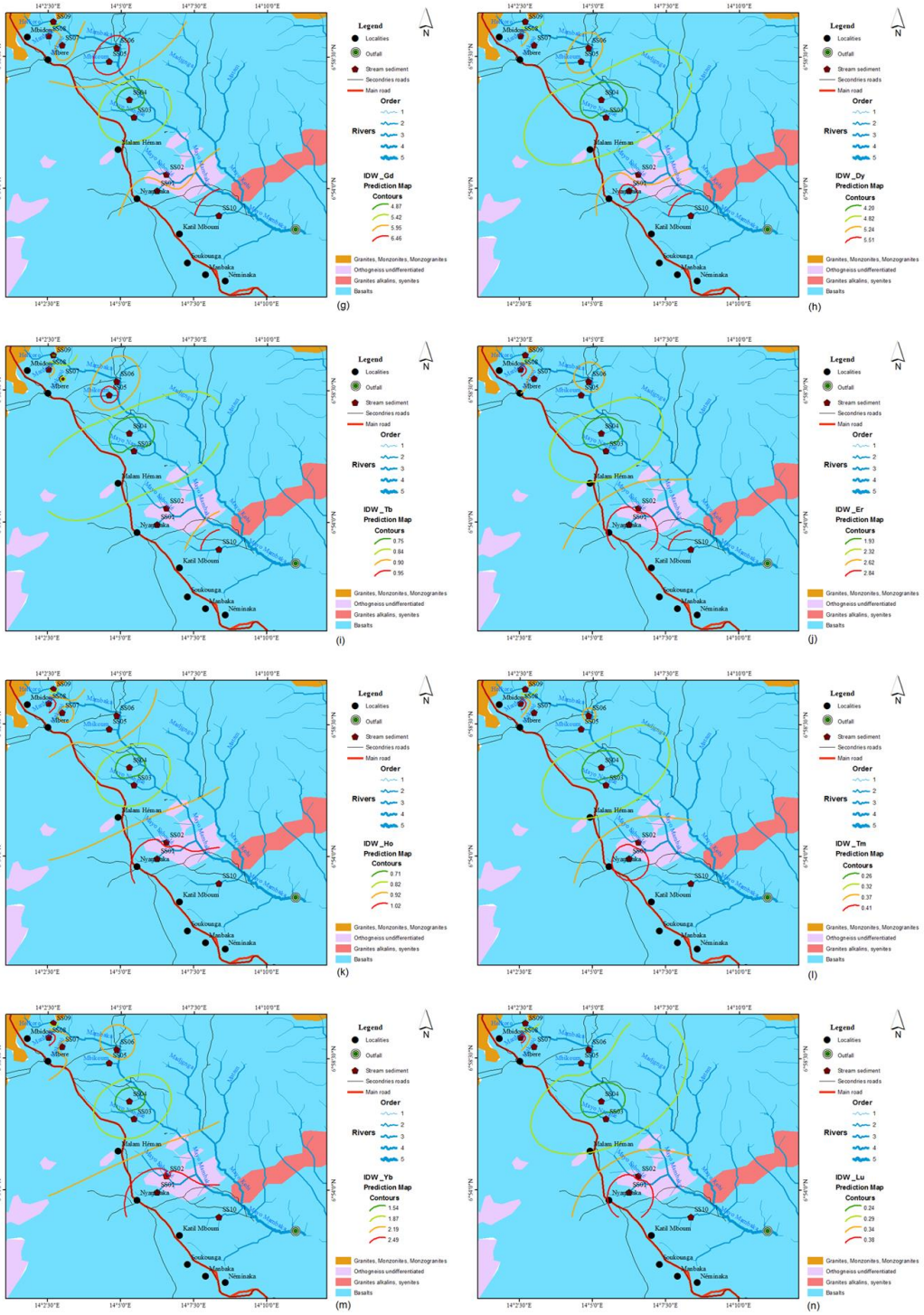

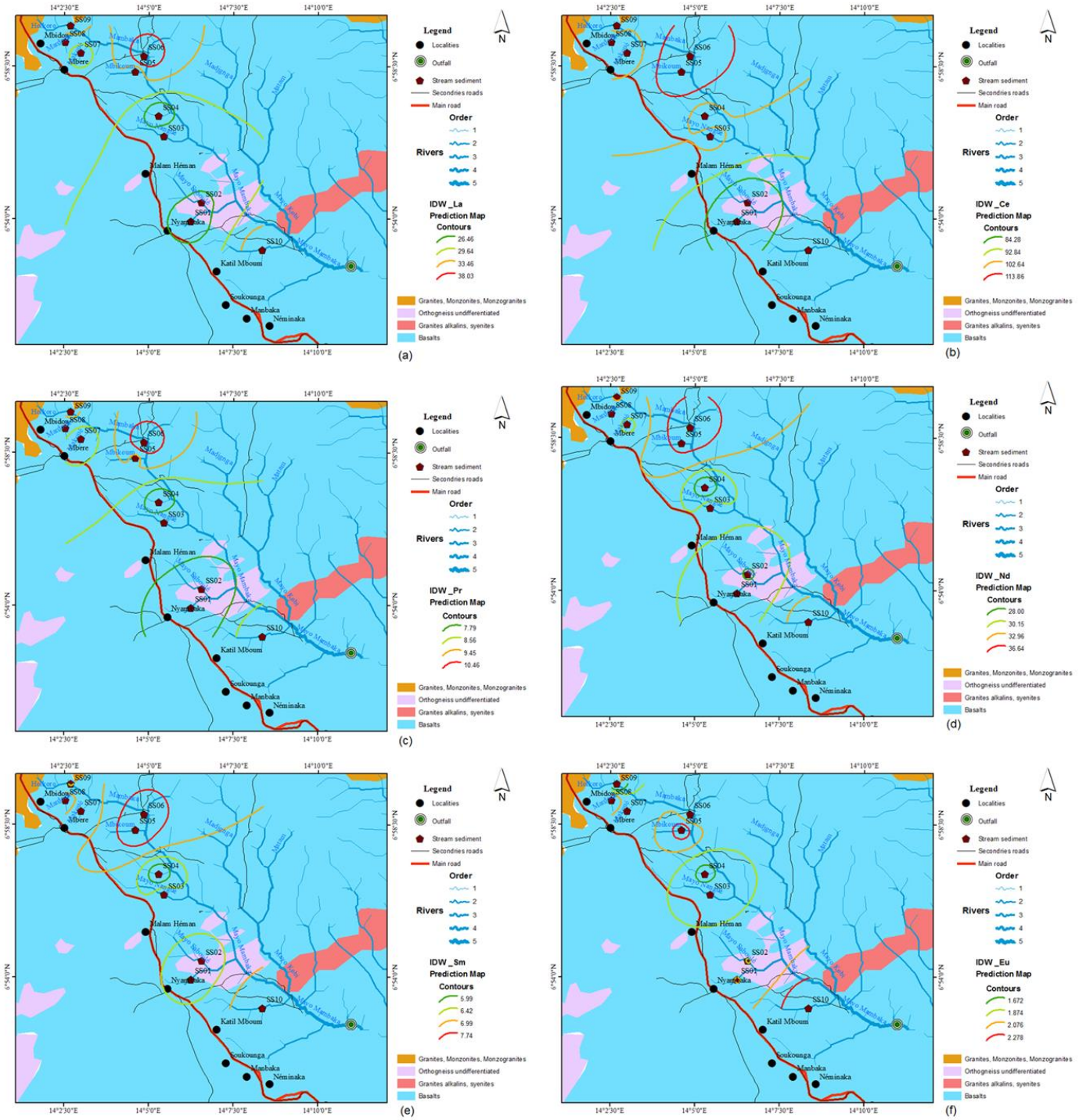

References

[1] *Kanazawa, Y., Kamitani, M. Rare earth minerals and resources in the world. Journal of Alloys and Compounds, 2006;* 408*: 1339-1343.*

[2] *Ling, Q., Liu, C. Review of Rare Earths and fluid-rock interaction. Journal of Rare Earths, 2002;* 20*(6): 570-578.*

[3] *Picard, S., Lecuyer, C., Barrat, J.A., Garcia, J.P., Dromart, G., Sheppard, S.M.F. Rare earth element contents of Jurassic fish and reptile teeth and their potential relation to seawater composition (Anglo-Paris Basin, France and England). Chemical Geology, 2002;* 186*(1-2): 1-16.*

[4] *Addy, S.K. Rare earth element patterns in manganese nodules and micronodules from Northwest Atlantic. Geochimica et Cosmochimica Acta, 1979;* 43*(7): 1105-1115.*

[5] *Watson, E.B., Green, T.H. Apatite/liquid partition coefficients for the rare earth elements and strontium. Earth and Planetary Science Letters, 1981;* 56*: 405-421.*

[6] *Yuan, F., Zhou, T., Yue, S. Study on mechanism of formation of volcanic rock in North Altay by using Rare Earths. Journal of Rare Earths, 2003a;* **21***(3): 387-390.*

[7] *Yuan, F., Zhou, T., Yue, S., Zhu, G., Hou, M. Rare Earths of magmatic rocks in Yanshanian Stage in adjacent region of Anhui and Jiangxi Provinces, Jiangnan uplift. Journal of Rare Earths, 2003b;* 21*(5): 591-594.*

[8] *Aide, M., Smith-Aide, CAssessing soil genesis by Rare-Earth elemental analysis. Soil Science Society of America Journal, 2003;* **67***(5): 1470-1476.*

[9] *Kirwood, C., Cave, M., Beamish, D., Grebby, S., Ferreira A. A machine learning approach to geochemical mapping. Journal of geochemical Exploration, 2016; 167, 49-61.*

[10] *Ling Q. and Liu C. Review of Rare Earths and fluid-rock interaction. Journal of Rare Earths (2002).* 20*(6): 570-578.*

[11] Toteu, S.F., Penaye, J., Poudjom Djomani, Y. Geodynamic evolution of the Pan- African belt in central Africa with special reference to Cameroon. Can. J. Earth Sci, 2004; 41, 73-85.

[12] Dumont, J.F. Étude structurale des bordures nord et sud du plateau de l'Adamaoua : influence du contexte atlantique. Géodynamique, 1987; 2, 55 – 68.

[13] Le Marechal, A., Vincent, P.M. Le fossé crétacé du Sud Adamaoua, Cameroun, in : T. F. J. Dessauvagie, A. J. Whiteman, (Eds.), African Geology, University of Ibadan,1970; 229 – 249.

[14] Popoff, M. The African rift system: basins, magmatism and rifting in the Benue trough, In : C. Coulon, A. B Kampunzu, R. T Lubala, (Eds), Mesozoïc to present day magmatism of the African plate and its structural setting, CIFEG, Paris, 1988.

[15] Tchakounté, J.N., Toteu, S.F., Van Schmus, R.W., Penaye, J., Deloule, É., Mvondo Ondoua, J., Houketchang M.B., Ganwa, A.A., White, W.M. Evidence of ca 1.6-Ga detrital zircon in the Bafia Group (Cameroon): Implication for the chronostratigraphy of the Pan-African Belt north of the Congo craton, C. R. Geoscience, 2007; 339 132–142.

[16] Tchamani, R., Pouclet, A., Penaye, J., Ganwa, A.A., Toteu, S.F. Petrography and geochemistry of the Ngaoundéré pan-African granitoïds in Central North Cameroon : implication for their sources and geological setting. Journal of African Earth Sciences, 2006; 44, pp. 511-529.

[17] Vicat, J.P., Ngounouno, I., Pouclet, A. Existence of old dolerites dykes of continental tholeïtes composition in the alkaline province of the Cameroon Line: Implication to the geodynamic context. Compte Rendu de l'Académie des Sciences (in French), Paris, Sciences de la Terre et des planètes / Earth and Planetary Sciences, 2001; 332, 243–249.

[18] Toteu, S.F., Penaye, J., Deloule, E., Vanschmus, W.R., Tchameni, R. Diachronous evolution of volcano sedimentary basins north of the Congo craton: from U-Pb ion microprobe dating of zircons from the Poli, Lom and Yaoundé Groups, Cameroon. Journal of African Earth Sciences, 2006; 44, 428 – 442.

[19] Ganwa, A.A., Frisch, W., Siebel, W., Ekodeck, G.E., Cosmas, S.K., Ngako, V.V. Archean inheritances in the pyroxene-amphibole-bearing gneiss of the Meiganga area, Central North Cameroon: Geochemical and 207Pb/206Pb age imprints. Comptes Rendus Géoscience, 2008; 340, 211 – 222.

[20] Diguim, A.K., Ganwa, A.A., Klötzli, U., Hauzenberger, C., Ngounouno, I., Naïmou, S. The Pan African Biotite-Muscovite Granite and Amphibole-Biotite Granite of Doua, Central Cameroon: Zircon Features, LA-MC-ICP-MS U-Pb Dating and Implication on Their Tectonic Setting. Journal of Geosciences and Geomatics, 2017; 5 (3) 119 – 129.

[21] Soba, D., Michard, A., Toteu, S.F., Norman, D.I., Penaye, J., Ngako, V., Nzenti, J.P., Dautel, D. Données géochronologiques nouvelles (Rb-Sr, U-Pb et Sm-Nd) sur la zone mobile panafricaine de l'Est Cameroun : âge protérozoïque supérieur de la série de Lom. Comptes Rendus de l'Académie des Sciences Paris, 1991; 312, 1453–1458

[22] Penaye J., Toteu SF, Tchameni, R., Van Schmus, W.R., Tchakounte, J., Ganwa, A., Minyem, D., Nsifa, E.N. The 2.1 Ga West central African Belt in Cameroon: extension and evolution. J Afr Earth Sci, 2004 ; 39:159–164.

[23] Cornacchia, M., Dars, R. Un trait structural majeur du continent africain : Les linéaments centrafricains du Cameroun au Golfe d'Aden. Bulletin de Société de Géologie, 1983; 2, 19 – 27.

[24] Moreau, C., Regnoult, M.J., Déruelle, B., Robineau, B. A new tectonic model for the Cameroon Line, central Africa. Tectonophysics, 1987; 139, 317 – 334.

[25] Saha Fouotsa, A.N., Tchaméni, R., Nomo, N.E., Dawai, D., Penaye, J., Fosso, T.P.M. Polyphase deformation in the Mbé - Sassa-Bersi area: implications on the tectono-magmatic history of the area and the tectonic evolution of the Tcholiré-Banyo and Central Cameroon Shear Zones, Central North Cameroon. Journal of Geosciences and Geomatics, 2018; 6 (2) 41 – 54.

[26] Fagny, A.M., Nkouandou, O.F., Bardintzeff, J.M., Temdjim, R., Guillou, H. Pétrologie du volcanisme Eocène Oligocène du massif de Tchabal Mbabo, Adamaoua-Cameroun, Afrique centrale. Afrique Science, 2016; 12 (6) 35 – 47.

[27] Nkouandou, O.F., Ngounouno, I., Déruelle, B., Ohnenstetter, D., Montigny, R.E.R. Petrology of the Mio-Pliocene Volcanism to the North and East of Ngaoundéré, Adamawa-Cameroon. Comptes Rendus Géoscience, 2008; 340, 27 – 38.

[28] Toteu, S.F., Van Schmus, R.W., Penaye, J. and Michard, A. New U-Pb and Sm-Nd Data from North Central Cameroon and Its Bearing on the Pre-Pan-African History of Central Africa. Precambrian Research, 2001; 108, 45-73. https://doi.org/10.1016/S0301-9268(00)00149-2.

[29] Nguetnkam, J.P., Yongue-Fouateu, R., Bitom, D., Bilong, P., Volkoff, B. Etude pétrologique d'une formation latéritique sur granite en milieu tropical forestier sud-camerounais (Afrique centrale). Mise en évidence de son caractère polyphasé. Etude et Gestion des Sols, 2006; 13, 89–102.

[30] Sepwouo S.A.D.S., Kouankap N.G.J., Mvodo H., Pemba N.S., Kamguia W.B., Nzenti J.P. Petrography and geophysical characterization of the newly discovery iron ore deposit in Mankoure (Bidou-East), Nyong group, South Cameroun. Result in geophysical Sciences, 2022; 12 100050.
[31] Sepwouo, S.A.D.S., Kouankap, N.G.J., Evine, L.N.T., Njikeu, O., Ngouem, P.A., Kamguia, K.M.S., Gukwa, S., Robillard, C., Nzenti, J.P. Alluvial gold particles microchemistry and induced polarization geophysical surveys in Makouré area, Nyong group, Cameroon: Constrain of orogenic gold prospectivity, 2023; ISSN en ligne 1866-7538
[32] Embui, V.F., Omang, B.O., Che, V.B., Nforba, M.T., Suh, E.C. Gold grade variation and stream sediment geochemistry of the the Vaimba-Lidi drainage system, northern Cameroon. Nat Sci, 2013; 5(2A):282–290.
[33] Mimba, M.E., Nforba, M.T., Suh, C.E. Geochemical dispersion of gold in stream sediments of the Paleoproterozoic Nyong Series, southern Cameroon. Sci Res, 2014; 2(6):155–165.
[34] Ongboye, P.R.B., Sababa, E., Bidzang, F.N., Ndjigui, P.D. Geochemical characterization of surface sediments from Tongo Gandima (Eastern Cameroon): implications for gold exploration, 2019; https://doi.org/10.1007/s12517019-4812-3.
[35] Edima, Y.R., Bidjo, E.G., Okomo, A.C., Ondoua, O.J. Stream Sediments Geochemistry of the Nyambaka Drainage System Northern Cameroon (Central Africa): A Target for Mining. International Journal of Statistical Distributions and Applications, 2021; 7(2): 25-34.
[36] Edima, Y.R., Balla, O.G., Fagny, M.A., Ekoa, B.A., Nkouandou, O.F. Mining Implication in the geochemical exploration of fluvial Sediment of the East Nyambaka Volcanic Zone (Adamawa-Cameroon). International Journal of Geosciences, 2022; 13, 361-381.
[37] Harris, R.J. A Primer of Multivariate Statistics. Psychology Press, 2001.
[38] Rencher, A.C. Methods of Multivariate Analysis. John Wiley & Sons, 2003; Vol. 492.
[39] Wold, S., Esbensen, K., Geladi, P. Principal component analysis. Chemometr. Intell. Lab. Syst, 1987; 2, 37–52
[40] Fabrigar, L.R., Wegener, D.T. Exploratory Factor Analysis. Oxford University Press, 2011.
[41] Carranza, E.J.M. Geochemical Anomaly and Mineral Prospectivity Mapping in GIS. Elsevier, 2008.
[42] Reimann, C., Filzmoser, P., Garrett, R., Dutter, R. Statistical Data Analysis Explained: Applied Environmental Statistics with R. John Wiley & Sons, Chichester, 2008; p. 362
[43] Zuo, R. Identifying geochemical anomalies associated with Cu and Pb–Zn skarn mineralization using principal component analysis and spectrum–area fractal modeling in the Gangdese Belt, Tibet (China). J. Geochem. Explor, 2011; 111, 13–22.
[44] Parsa, M., Maghsoudi, A., Carranza, E.J.M., Yousefi, M. Enhancement and mapping of weak multivariate stream sediment geochemical anomalies in Ahar Area, NW Iran. Nat. Resour. Res, 2017a; 26, 443–445.
[45] Parsa, M., Pour, A.B. A simulation-based framework for modulating the effects of subjectivity in Greenfield Mineral Prospectivity Mapping with geochemical and geological data. J. Geochem. Explor (2021), 229, 106838.
[46] Zuo, R., Xiong, Y. Geodata science and geochemical mapping. J. Geochem. Explor, 2020; 209, 106431.
[47] Rudnick, R.L., Gao, S. The Composition of the Continental Crust. In: Holland H.D., Turekian K.K., Eds., Treatise on Geochemistry, 3, the Crust, Elsevier-Pergamon, Oxford, 1 64 slate in Baiyun'ebo mine, Inner Mongolia. Geoscience, 2003; 17, 281–286.
[48] Yang, X., Zhu, M., Zhao, Y., Zhang, J., Guo QPi, D. REE geochemical characteristics of the ediacaran-lower cambrian black rock series in Eastern Guizhou. Geol. Rev, 2008; 54, 3-15.
[49] Ji, H., Ouyang, Z., Wang, S., Zhou, D. Element geochemistry of weathering profile of dolomitite and its implications for the average chemical composition of the upper-continental crust. Sci. China Ser, 2000; D, 43, 23–35.
[50] Gas'kov, I.V., Tran, T.A., Tran, T.H., Pham, T.D., Nevol'ko, P.A., Pham, N.C. The Sin Quyen Cu–Fe–Au–REE deposit (northern Vietnam): composition and formation conditions. Russian Geology and Geophysics, 2012; 53 442–456.
[51] Huang, X.W., Mei-Fu, Z., Yu-Zhuo, Q., Liang, Q. In-situ LA-ICP-MS trace elemental analyses of magnetite: The Bayan Obo Fe-REE-Nb deposit, North China. Ore Geology Reviews, 2015; 65, 884–899.
[52] Xiao, R., Shi, S., An, G., Zhang, H., Fei, H. Genetic characteristic of hydrothermal sedimentation of k-rich, 2003.
[53] *Compton, J.S., White, R.A., Smith, M. Rare earth element behavior in soils and salt pan sediments of a semi-arid granitic terrain in the Western Cape, South Africa. Chemical Geology, 2003;* 201*(3-4): 239-255.*
[54] *Galán, E., Fernández-Caliani, J.C., Miras, A., Aparicio, P., Márquez, M.G. Residence and fractionation of rare earth elements during kaolinization of alkaline peraluminous granites in NW Spain. Clay Minerals, 2007;* 42*(3): 341-352.*
[55] *Nagasawa, H. Partitioning of Eu and Sr between coexisting plagioclase and K-feldspar. Earth and Planetary Science Letters, 1971;* 13*(1): 139-144*
[56] *Panahi, A., Young, G.M., Rainbird, R.H. Behavior of major and trace elements (including REE) during Paleoproterozoic pedogenesis and diagenetic alteration of an Archean granite near Ville Marie, Quebec, Canada. Geochimica et Cosmochimica Acta, 2000;* 64*(13): 2199-2220*
[57] *Aubert, D., Stille, P., Probst, A., Gauthier-Lafaye, F., Pourcelot, L., Del Nero, M. Characterization and migration of atmospheric REE in soils and surface waters. Geochimica et Cosmochimica Acta, 2002;* 66*(19): 3339-3350.*
[58] *Hu, Z., Haneklaus, S., Sparovek, G., Schnug, E. Rare earth elements in soils. Communications in Soil Science and Plant Analysis, 2006b;* 37*(9/10): 1381-1420.*